Structural and Electrical Conductivity Studies of Spinel $Li_4Ti_5O_{12}$ Anode Thin Films Grown by RF Magnetron Sputtering

Kamatam Hari Prasad [a, b], Ratnakar Arumugam [a, c], E.S. Srinadhu [d], N. Satyanarayana [a, *]

[a]Department of Physics, Pondicherry University, Puducherry – 605014, India.
[b] Institute of Aeronautical Engineering, Dundigal, Hyderabad – 500 043, India.
[c] Centre for Nanoscience and Technology, Pondicherry University, Puducherry – 605014, India.
[d] LAM Research Corporation, Fremont, CA, 94538, USA
*Corresponding author. Tel: 0413-2654404; E-mail: nallanis2011@gmail.com

ABSTRACT

Spinel $Li_4Ti_5O_{12}$ (LTO) thin films were deposited on Ti/Si (100) substrate by an RF magnetron sputtering method at ambient temperature and followed by annealing at 400, 500 and 600 ºC under an oxygen atmosphere. The observed X-ray diffraction pattern of annealed at 600 ºC LTO thin film showed the formation of cubic spinel phase. AFM micrographs of LTO thin films reveal their surface morphology and roughness. The conductivity of annealed at 600 ºC LTO thin film is evaluated by analyzing the measured impedance data using the win fit software and it is found to be 5.47×10^{-6} S cm^{-1}. The ac conductivity of the as-deposited and post-annealed LTO thin films was evaluated using the measured impedance data as a function of temperature and frequency (100 Hz to 10 MHz) and it is found to increase with a rise of annealing temperatures. Hence, the observed results of the developed annealed LTO thin film at 600 ºC can be a better anode material for developing all-solid-state rechargeable high energy density lithium-ion micro-batteries.

Keywords: RF Magnetron Sputtering; $Li_4Ti_5O_{12}$ thin films; XRD, AFM, impedance, DC and AC conductivities.

1. INTRODUCTION

All-solid-state rechargeable batteries with high energy density are the most promising energy storage devices for electric vehicles and other portable electronic devices. Among the available energy sources, lithium-ion (Li-ion) batteries are more suitable, since these not only exhibit high power and high energy density but also miniaturization of battery technology is possible [1-6]. Li-ion micro-batteries can be utilized in various microsystems applications such as micro-sensors, micro-mechanics, microelectronics, etc. In order to realize such micro-batteries, developing thin-film technology is very important. Spinel $Li_4Ti_5O_{12,}$ (LTO) is found to be a potential candidate as an anode material for rechargeable Li-ion batteries because of the following properties [7-10]. Good Li-ion intercalation and de-intercalation reversibility, no structural change during charge-discharge cycling, zero-strain effect, good safety characteristics, thermal stability, etc. Hence, in the present investigation, the structural and electrical conductivity of $Li_4Ti_5O_{12}$ thin films grown by rf magnetron sputtering were studied to find out its suitability for developing all-solid-state thin-film Li-ion micro-batteries.

In the present investigation, spinel LTO thin films are deposited on Ti/Si (100) substrate by RF magnetron sputtering. All the deposited LTO thin films are characterized using XRD, and AFM techniques. Also, the dc and ac conductivities were evaluated by analyzing the measured impedance data using the win fit software of LTO thin films of as-deposited and post-annealed at different temperatures as a function of frequencies.

2. EXPERIMENTAL TECHNIQUES

2.1 Preparation of $Li_4Ti_5O_{12}$ thin films

High purity (99.99%) spinel LTO target (50.88 mm diameter and thickness of 3 mm) bonded with the copper backing plate, the (100) oriented silicon (Si) substrate of thickness 0.125 mm were obtained from Testbourne Pvt. Ltd., USA. $Li_4Ti_5O_{12}$ (LTO) thin films were deposited via the 'sputter-down' configuration at ambient temperature using the radio frequency (RF: 13.56 MHz) magnetron sputtering system (Milman Thin Film System Pvt. Ltd, India) with maximum output power of 600 W. During RFMS process, the rise in substrate temperature due to self-heating in plasma is monitored by a thermocouple. Initially, Si substrates were cleaned in the ultrasonic bath using solvents like pure acetone, isopropanol and deionized water for 15 min., respectively and dried under a nitrogen atmosphere. As obtained LTO target was fixed to the magnetron, and the distance between Si substrate and LTO target was fixed at 15 cm. A turbomolecular and rotary, as the backup, pumps were used to obtain the chamber base pressure of 1×10^{-7} Torr and then passed ultra-high pure Ar gas into the chamber through mass flow controller. The pre-sputtering process was performed for about 15 min. to remove surface contamination on LTO target and on Si substrate. Prior to the deposition of LTO material, a thin titanium (Ti) film of ~ 25 nm was sputtered onto Si substrate to serve as an adhesive layer. Then LTO thin films were deposited on Ti/ (100) oriented silicon (Si) substrates by using RFMS power of 100 W at room temperature under an

argon atmosphere at 1×10^{-3} Torr pressure. The thickness of the deposited LTO thin films was measured using a quartz crystal thickness monitor and it is found to be 100 nm. The as-deposited LTO films were annealed at different temperatures 400, 500 and 600 ºC in a pure oxygen atmosphere.

2.2 CHARACTERIZATION

XRD patterns of LTO films were recorded using the PANalytical, Philips, X' Pert Pro X-ray diffractometer having monochromatic X-ray source of CuK_α radiation with a wavelength (λ) of 1·541060 Å, operated at 40 kV and 30mA. Atomic Force Microscopy (AFM) images of the LTO films were acquired using the Nano Scope-V Multimode™ SPM, Veeco Instruments and all the acquired LTO films were examined to find out their surface morphology. The AFM was operated in tapping mode (non-contact) to prevent the damage to the films and also to provide optimal image and quality data. From the 3-D AFM micrographs of the LTO thin films, grain shape, size and surface roughness parameters like root mean square (RMS) roughness (R_q), average surface roughness (R_a) are determined using Nano scope analysis software. The impedance data of the as-deposited and post-annealed samples at different temperatures of LTO thin films [(Cu)/($Li_4Ti_5O_{12}$/Ti/Si(100)/(Cu)] were measured in the frequency range from 100 Hz to 10 MHz using Alpha A high-performance frequency analyzer of Novocontrol, Germany. The measured impedance data were analyzed using the win fit software and evaluated the resistance of all the prepared LTO thin films. Conductivity (σ_{dc}) of LTO thin films was calculated using the evaluated the resistance and the dimensions of LTO thin films and also AC conductivity (σ_{ac}) of LTO thin films was calculated using the measured impedance data and the dimensions of LTO thin films.

3. RESULT AND DISCUSSION

3.1 XRD

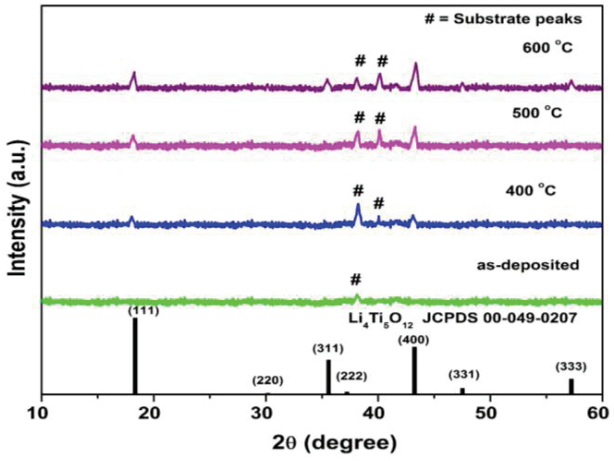

Fig. 1. X-ray diffraction patterns of as-deposited and annealed at various temperatures of LTO thin films along with the standard JCPDS data

From fig. 1, it is observed that the X-ray diffraction pattern of the as-deposited LTO thin film possesses poor crystalline nature with a low intensity of diffraction peak at 2θ = 38.20º corresponding to the reflection from (002) plane of the substrate (Si). From fig. 1, for the annealed at 400 ºC of LTO thin film showed new XRD peaks at 2θ = 18.40º, and 43.30º. The intensity of the XRD peaks increases with the increase of annealing temperature up to 600 ºC. From fig.1, the LTO thin film annealed at 600 ºC showed the most prominent XRD peak at 2θ = 43.30º, which corresponds to the reflection from (400) plane. Apart from this, four other observed XRD peaks at 2θ = 18.40º, 35.5º, 47.40º, and 57.20º were compared with the JCPDS (card no. 49-0207) data and respectively assigned to the reflections from (111), (311), (331) and (333) planes, which confirm the formation of crystalline cubic spinel $Li_4Ti_5O_{12}$ phase. The XRD peak marked as '#' is due to the Ti/Si (100) substrate. From fig.1, It also observed that the intensity of the XRD peaks is increasing with improved sharpness as well as with a slight shift in peak positions toward the lower diffraction angle. Hence, the observed XRD results of the LTO films indicate that the crystallization of the films is improved with the increase of annealing temperature.

3.2 AFM

From fig. 2. [a, b, c, d]], the AFM images clearly show that the grain size increases with post-annealing temperature. From fig. 2 [a], the 3D AFM image of the as-grown LTO film shows smaller individual grain with low roughness. From fig. 2. [b, c, and d], 3D AFM micrographs of the post-annealed (at 400 ºC, 500 ºC, and 600 ºC) LTO thin films show denser granular structure. It is also observed that there is a decrement in the separation between the grains and grain boundary increases with the increase of temperature. From AFM images, the grain size, R_a, and R_q values were evaluated using Nanoscope analysis software and are presented in table 2. From table 1, it is observed that the grain sizes are found to be 37 nm, 49 nm, 85 nm, and 98 nm, respectively for the as-deposited and post-annealing temperatures at 400 ºC, 500 ºC and 600 ºC of LTO films, which indicate that the grain size increases with increasing of post-annealing temperature [7]. The grain size plays an important role in the electrochemical performance of Li-ion batteries, because, the small grain size can provide the large specific surface area, shorter Li-ion diffusion path and easy to migrate the Li-ions from in and out of the spinel LTO system. From table 2, it is also found that the post-annealed at 600 ºC of LTO film has the highest surface roughness (R_a: 18 nm and R_q: 16.6 nm) and the as-grown LTO thin film has the smallest surface roughness (R_a of 1.55 nm and R_q of 1.92 nm).

Table 2:

Temperature (°C)	Average roughness (nm) R_a	RMS roughness (nm) R_q	AFM grain size (nm)
As-deposited	1.55	1.92	37
400 ºC	2.14	2.78	49
500 ºC	14	11	85
600 ºC	18	16.6	98

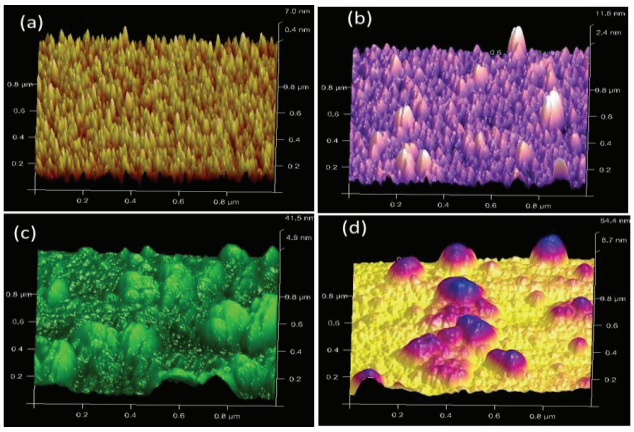

Figure 2: 3-dimensional AFM micrographs of the LTO thin films of [**a]** as-deposited, and post-annealed at [**b]** 400 ºC, **[c]** 500 ºC, and **[d]** 600 ºC.

3.3. Impedance Spectroscopy

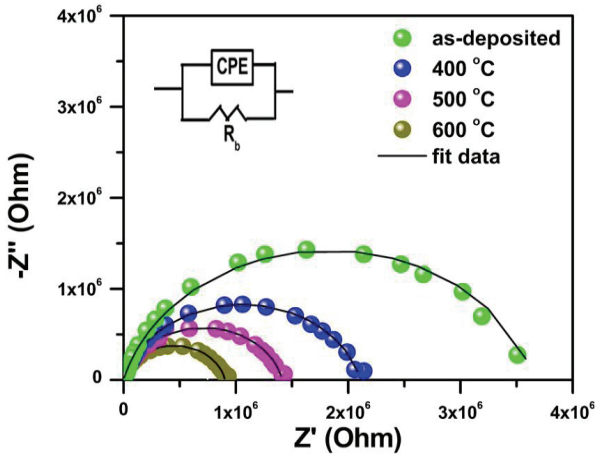

Fig. 3. Impedance plots obtained at room temperature of LTO thin films of as-deposited and post-annealed at different temperatures (400 ºC, 500 ºC, and 600 ºC).

Fig. 3, shows the Nyquist plots (imaginary (-Z″) vs. real (Z′)) obtained at room temperature of LTO thin films of as-deposited and post-annealed at different temperatures (400 ºC, 500 ºC, and 600 ºC). From fig. 3, observed the impedance plots of LTO thin films of as-deposited and post-annealed at different temperatures show the single depressed semicircle in the measured frequency range. From fig. 3, it is also observed that the centers of the semicircles are below the real axis (Z′) and shift towards the origin with a rise in annealing temperature. It is also clearly seen from the figures that the radius of the semicircle decreases with the increase of annealing temperature. Further, it is also observed that the frequency at which imaginary part (-Z″) attains the maximum is also shifted towards the higher frequencies with the increase of annealing temperature. This indicates that the resistance of LTO thin film decreases with the increase of annealing temperature, which in turn, increases the conductivity of LTO thin film sample with the increase of annealing temperature. The measured impedance data of LTO thin film of as-deposited and post-annealed at different temperatures of LTO samples were analyzed by using winfit software and obtained resistance (R) and its electrical behavior, in terms of the equivalent circuit, as shown in the inset of fig. 3. The formation of single semicircle corresponds to the parallel combination of constant phase element (CPE) and resistance of the LTO thin film. The resistance obtained from impedance plot and the sample dimension are used to calculate the electrical conductivity (σ) of the LTO thin film samples, by using the following equation [7-16]

$$\sigma = \frac{1}{R}\frac{t}{A} \qquad (1)$$

Where σ is the electrical conductivity of the LTO thin film, t is the thickness of the LTO thin film, A is the area of the LTO thin film, and R is the resistance of the LTO thin film. The observed electrical conductivity of the LTO thin film samples is found to be 4.40 x 10^{-8} S cm^{-1} and 5.47×10^{-6} S cm^{-1} respectively at as-deposited and post-annealed at 600 ºC.

3.4. AC conductivity (σ_{ac})

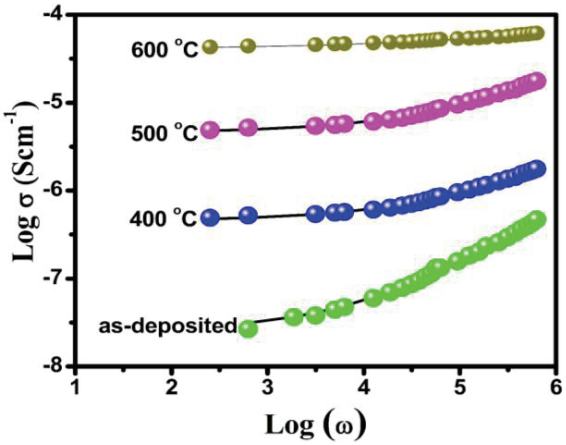

Fig. 4. The Log (σ) vs. Log (ω) plots obtained at room temperature of LTO thin films of as-deposited and post-annealed at different temperatures (400 ºC, 500 ºC, and 600 ºC).

Fig. 4 shows the Log (σ) vs. Log (ω) plots obtained at room temperature of LTO thin films of as-deposited and post-annealed at different temperatures (400 ºC, 500 ºC, and 600 ºC). From fig. 4, the frequency dependent conductivity plots showed two distinct regions within the measured frequency window, (i) the low-frequency plateau region and (ii) high-frequency dispersion region. The plateau region corresponds to frequency independent conductivity $\sigma_{(0)}$ or dc conductivity (σ_{dc}) and it is evaluated by extrapolating the plateau region to the zero frequency (Y-axis). The frequency independent conductivity may be attributed to the long-range transport of free charge carriers with the applied field in LTO thin films. The observed a.c. conductivity in the high-frequency dispersion region follows Jonscher's universal power law (JUPL) [7-16].

$$\sigma_{(\omega)} = \sigma_{(0)} + A\omega^{s} \qquad (2)$$

TechConnect Briefs 2018, TechConnect.org, ISBN 978-0-9988782-3-2

where, $\sigma_{(\omega)}$ is the ac conductivity, $\sigma_{(0)}$ is the zero frequency limit of $\sigma_{(\omega)}$, A is a constant, and *s* is the power law exponent ($0 < s < 1$).

From fig.4, it can be observed that the frequency at which the dispersion region deviated from the plateau is defined as the hopping frequency (ω_p), where, the relaxation effects starts. Also, it can be observed that the hoping frequency moved towards the higher frequency with the increase of temperature in the LTO thin film is due to hopping of charge carriers between adjacent sites, results in local displacement of charge carriers in the direction of the applied frequency. Hence, the observed dispersion region of conductivity curves may follow the diffusion controlled relaxation (DCR) model [7-16].

4. CONCLUSION

Nanocrystalline spinel $Li_4Ti_5O_{12}$ (LTO) thin films were grown at room temperature by RF magnetron sputtering on Ti/ (100) oriented silicon (Si) substrate and annealed at different temperatures up to 600 ^oC under an oxygen atmosphere. The phase purity of the LTO films was confirmed by X-ray diffraction result. The surface morphology and roughness of the LTO films were obtained from AFM results. The electrical conductivity of the LTO thin film deposited under an argon atmosphere and post-annealed at 600 ^oC is evaluated by analyzing the measured impedance data using the win fit software and it is found to be 5.47×10^{-6} S cm^{-1}. The ac conductivity (σ_{ac}) of the as-deposited and post-annealed LTO thin films was evaluated using the measured impedance data as a function of temperature and frequency (100 Hz to 10 MHz) and the evaluated ac conductivity (σ_{ac}) is found to increase with a rise of annealing temperatures of LTO thin film. Based on the above observed results, the developed annealed LTO thin film at 600 ^oC may provide a great prospect as an anode material for developing all-solid-state rechargeable high energy density lithium-ion micro-batteries.

ACKNOWLEDGMENT

NS would like to thank the DST-Nano mission, Govt. of India, for providing grants in the form of research project sanction letter No.: SR/S5/NS-49/2005, dated on 30-07-2010 and NRB-DRDO, Govt. of India, for providing grants in the form of research project sanction letter No.: NRB-377/MAT/16-17, dated on 19-04-2016, respectively for developing five targets DC/RF magnetron sputtering system and electrochemical system facilities for developing and characterizing all solid state thin film lithium ion micro-batteries.

REFERENCES

[1] J. M. Tarascon, M. Armand, Nature, 414 (2001) 359-367.
[2] M. M. Thackeray, W. I. F. David, P. G. Bruce, J. B. Goodenough, Mater. Res. Bull., 18 (1983) 461-472.
[3] D. K. Kim, P. Muralidharan, H. W. Lee, R. Ruffo, Y. Yang, C. K. Chan, H. Peng, R. A. Huggins, Y. Cui, Nano Lett., 8 (11) (2008) 3948-3952.
[4] J. Feng, X. Gao, L. Cia, S. Xiong, RSC Adv., 6 (2016) 7224-7228.
[5] J. Wang, Y. Li, X. Sun, Nano Energy, 2 (2013) 443-467.
[6] A. Ratnakar, K. Hari Prasad, S Vivekananthan, P C Karthika, Aashutosh Kumar, Material Today: Proceedings, 3(10) (2016) 4052-4057.
[7] Kamatam Hari Prasad, S. Vintoth, P. Jena, M. Venkateswarlu, N. Satyanarayana, Materials Chemistry and Physics, **194** (2017) 188-197.
[8] Kamatam Hari Prasad, S. Subramanayam, T.N. Sai ram, G. Amarendra, E.S. Srinadh, N. Satyanarayana, Journal of Alloys and Compounds, **718** (2017) 459-470.
[9] K. Hari Prasad, A. Ratnakar, Aashutosh Kumar, N. Satyanarayana, Material Today: Proceedings, **3(10)** (2016) 4064-4069.
[10] Paramananda Jena, N. Nallamuthu, K. Hariprasad, M. Venkateswarlu, N. Satyanarayana, Journal of Sol-gel Science and Technology, **72** (2014) 480-489.
[11] K. Hari Prasad, N. Naresh, B. Nageswar Rao, M. Venkateswarlu, N. Satyanarayana, Material Today: Proceedings, **3(10)** (2016) 4040-4045.
[12] K. Hari Prasad, P. Muralidharan, E.S. Srinadhu, N. Satyanarayana, Advanced Materials-TechConnect Briefs 2017, 2 (2017) 106-109.
[13] K. Hari Prasad, P. Muralidharan, E.S. Srinadhu, N. Satyanarayana, Advanced Materials - TechConnect Briefs 2017, 2 (2017) 90-93.
[14] K. Hari Prasad, P. Muralidharan, E.S. Srinadhu, N. Satyanarayana, Advanced Materials - TechConnect Briefs 2017, 2 (2017) 114-117.
[15] K. Hari Prasad, S. Vinoth, A. Ratnakar, N. Satyanarayana, Material Today: Proceedings, **3(10)** (2016) 4046-4051.
[16] P. Muralidharan, N. Nallamuthu, I. Prakash, N. Satyanarayana, J. Am. Ceram. Soc., 90 (2007) 125-131.